Title
Understanding the dynamic relationship between cerebral blood flow and the BOLD signal: Implications for quantitative functional MRI

Permalink
https://escholarship.org/uc/item/0fk4p4gf

Authors
Simon, Aaron B
Buxton, Richard B

Peer reviewed

Understanding the dynamic relationship between cerebral blood flow and the BOLD signal: Implications for quantitative functional MRI

Aaron B. Simon[a] and **Richard B. Buxton**[b],*

[a]Department of Bioengineering, University of California San Diego, La Jolla, CA 92093, USA

[b]Department of Radiology and Center for Functional Magnetic Resonance Imaging, University of California San Diego, La Jolla, CA, 92093, USA

Abstract

Calibrated BOLD imaging, in which traditional measurements of the BOLD signal are combined with measurements of cerebral blood flow (CBF) within a BOLD biophysical model to estimate changes in oxygen metabolism ($CMRO_2$), has been a valuable tool for untangling the physiological processes associated with neural stimulus-induced BOLD activation. However, to date this technique has largely been applied to the study of essentially steady-state physiological changes (baseline to activation) associated with block-design stimuli, and it is unclear whether this approach may be directly extended to the study of more dynamic, naturalistic experimental designs. In this study we tested an assumption underlying this technique whose validity is critical to the application of calibrated BOLD to the study of more dynamic stimuli, that information about fluctuations in venous cerebral blood volume (CBV_v) can be captured indirectly by measuring fluctuations in CBF, making the independent measurement of CBV_v unnecessary. To accomplish this, simultaneous arterial spin labeling and BOLD imaging was used to measure the CBF and BOLD responses to flickering checkerboards with contrasts that oscillated continuously with frequencies of ~0.02-0.16Hz. The measurements were then fit to a dynamic physiological model of the BOLD response in order to explore the range of consistent $CMRO_2$ and CBV_v responses. We found that the BOLD and CBF responses were most consistent with relatively tight dynamic coupling between CBF and $CMRO_2$ and a CBV_v response that was an order of magnitude slower than either CBF or $CMRO_2$. This finding suggests that the assumption of tight flow-volume coupling may not be strictly valid, complicating the extension of calibrated BOLD to more naturalistic experimental designs.

*Corresponding author at: University of California San Diego, 9500 Gilman Drive, MC 0677, La Jolla, CA 92093-0677, USA. Fax: +1 858 822 0605., rbuxton@ucsd.edu (R. B. Buxton).

1. Introduction

Because of the considerable energy demands of neuronal communication, neural activity in the brain is closely coupled to the regulation of local blood flow, allowing the brain to increase the delivery of glucose and oxygen in concert with electrical activity (Attwell and Laughlin, 2001; Iadecola, 2004). This link between neural and hemodynamic activity is exploited by Blood Oxygenation Level Dependent (BOLD) functional magnetic resonance imaging (fMRI), which uses changes in local blood deoxyhemoglobin as a biomarker for changes in neural activity (Ogawa et al., 1992). Though the physiological mechanism that links neural activity to deoxyhemoglobin is complex and incompletely understood, BOLD signal changes evoked by neural stimuli have consistently been shown to localize to areas determined to be functionally salient through invasive electrophysiological studies (Logothetis, 2008). The impressive precision with which BOLD imaging is capable of localizing changes in neural activity, as well as its non-invasive nature, have made BOLD imaging a valuable tool for investigating where in the brain cognitive functions are processed, especially in human beings.

However, using BOLD imaging to ask more than simply *where* the neural response to a stimulus takes place presents a challenge. Specifically, interpreting the magnitude of a BOLD signal change quantitatively as a metric of underlying neural activity is problematic. The fundamental difficulty in interpreting the BOLD signal quantitatively is that the local concentration of deoxyhemoglobin, to which the BOLD signal is sensitive, decreases in response to an increase in cerebral blood flow (CBF), but increases in response to an increase in venous blood volume (CBV_v) or oxygen metabolism ($CMRO_2$) (Buxton et al., 1998). Simple neural stimuli are generally thought to evoke an increase in all three of these variables, with CBF changes dominating such that deoxyhemoglobin decreases enough to be qualitatively detected by BOLD fMRI. However, the magnitude and dynamics of the BOLD signal change depend on all three of these variables and thus may not always be reflective of the underlying change in neural activity (Ances et al., 2008; Buxton, 2010; Griffeth et al., 2011; Moradi et al., 2012).

A promising solution to this problem of BOLD signal ambiguity has been to combine BOLD imaging with arterial spin labeling (ASL) measurements of CBF within a biophysical model of the BOLD effect in order untangle the physiological processes (e.g. CBF, $CMRO_2$) that link neuronal signaling to changes in MR signal decay via blood deoxyhemoglobin content (Davis et al., 1998). The idea behind this approach, termed calibrated BOLD imaging, is that while these variables may still be indirectly related to neural activity, they at least represent concrete, quantitative, and fundamentally physiological processes that can be compared across subjects, groups, and measurement techniques. To date, this approach has largely been applied to study physiological responses to simple neural stimuli presented in a block-design fashion. However, it would be highly useful to extend it to the study of more dynamic fluctuations in neural activity such as those associated with viewing naturalistic movies (Hasson, 2004), responding to internal stimuli (Smith et al., 2009), or even tracking transient pathological events such as cortical spreading depression (Hadjikhani et al., 2001), which are lately of increasing interest to both the basic and clinical neuroscience communities.

An important obstacle to applying the calibrated BOLD approach to the study of dynamic fluctuations in neural activity is our lack of understanding of the relative dynamics of the associated blood flow, blood volume, and oxygen metabolism changes. Observations of transient features of the BOLD response to simple stimuli suggest that these changes may not be dynamically coupled, at least under some experimental conditions. For example, observations of an "initial dip" in the BOLD signal immediately following the onset of stimulation are typically interpreted as evidence of the metabolic response preceding the hemodynamic response (Ances, 2004), while observations of a BOLD signal "post-stimulus undershoot" have been variously attributed to the slow recovery of blood volume (Buxton et al., 1998; Chen and Pike, 2009a) or oxygen metabolism (Donahue et al., 2009), or to a post-stimulus undershoot of blood flow (Chen and Pike, 2009a). In a block design experiment, these dynamics are relatively unimportant, as long, constant stimuli may be assumed to evoke physiological changes that reach an approximate steady state after a reasonable period of time. However, in a less constrained experiment in which neural activity is fluctuating continuously, these dynamics become critically important because they determine the number of variables that need to be measured in order to untangle the BOLD signal. A key assumption of the calibrated BOLD approach is that steady state changes in blood volume are directly related to changes in blood flow, eliminating the need to measure this variable independently in order to calculate changes in oxygen metabolism. If this assumption were invalid under more dynamic conditions, then more measurements would be needed to estimate $CMRO_2$ fluctuations than BOLD and ASL alone.

In order to better understand how the dynamics of CBF, CBV_v, and $CMRO_2$ affect the relationship between continuous ASL and BOLD time series, we examined the dynamic relationship between the fluctuations in CBF and the BOLD signal evoked in the human visual cortex by a fast flickering checkerboard (8 Hz) with a contrast that oscillated continuously and more slowly at several different temporal frequencies (~0.02 – 0.16 Hz). We hypothesized that if the dynamics of the CBF, $CMRO_2$, and CBV_v responses to the stimulus were different, then we would see cyclic changes in the relationship between CBF and the BOLD signal that would depend upon the frequency or phase of contrast oscillation. In order to relate deviations in the relationship between CBF and BOLD to the dynamics of the underlying physiological response, we fit our measurements to a dynamic model of the physiology underlying the BOLD response (Obata et al., 2004), finding that the measured responses to the stimulus were most consistent with a dynamically coupled CBF and $CMRO_2$ response and a CBV_v response that was an order of magnitude slower.

2. Theory

2.1 Static and dynamic models of the BOLD response

The BOLD phenomenon is a highly complex process (Buxton, 2013). Fluctuations in neural activity produce dynamic changes in oxygen metabolism, blood flow, and blood volume which, in turn, determine the quantity and distribution of deoxyhemoglobin in an imaging voxel at a given moment in time. Fluctuations in these parameters then produce changes in the decay rate of the signal that is ultimately measured in a BOLD experiment. Fortuitously, detailed biophysical models of the BOLD response suggest that, at least under quasi-static

conditions, the BOLD phenomenon can be remarkably well-approximated by much simpler heuristic models, which are used for calibrated BOLD analysis (Davis et al., 1998; Griffeth et al., 2013; Griffeth and Buxton, 2011). A useful heuristic model is the Griffeth model, which can be described by the equation

$$\delta b = A \times (1 - \alpha_v - 1/n) \times (1 - 1/(1 + \delta f)) \quad (1)$$

where δb is the measured fractional change in the BOLD signal, δf is the measured fractional change in CBF, α_v describes an assumed relationship between CBF and CBV_v changes based on previous experiments, and A is a scaling parameter related to baseline deoxyhemoglobin that is determined by a calibration experiment (Griffeth et al., 2013).This leaves n, which represents the ratio of fractional changes in CBF to $CMRO_2$ and is calculated from the measured data. In an experiment, δb and δf are sampled discretely in time, making it tempting to simply calculate n (or $CMRO_2$) as another discrete-time signal (Davis et al., 1998). This implicitly assumes that α_v is fixed, or equivalently, that CBF and CBV_v are tightly coupled dynamically.

In order to explore the potential physiological responses that could produce BOLD responses consistent with our measured data, we needed a BOLD signal model with more degrees of freedom than the steady state models typically used for calibrated BOLD analysis. We chose to work with an adaptation of the balloon model described by Obata et al. (Obata et al., 2004) because it is describable with a relatively small number of parameters and yet detailed enough to capture the effects of decoupled CBF, $CMRO_2$, and CBV_v dynamics, as well other features of a realistic vascular bed, such as a finite transit time for blood through the vasculature.

The model consists of a system of differential equations describing the changes in deoxyhemoglobin within a single, homogeneous venous compartment (where $q(t)$ denotes the ratio of deoxyhemoglobin content at time t to the baseline state) as the result of changes in $CMRO_2$ (where $r(t)$ denotes the ratio of $CMRO_2$ at time t to $CMRO_2$ in the baseline state), CBF (where $f_{in}(t)$ denotes the ratio of CBF at time t to CBF in the baseline state), and CBV_v (where v(t) denotes the ratio of CBV_v at time t to CBV_v in the baseline state). The equations governing the system are as follows:

$$dq/dt = (1/\tau_0) \times (r(t) - f_{out}(v, t) \times q(t)/v(t)) \quad (2)$$

where τ_0 represents the transit time for blood through the venous compartment and $f_{out}(v,t)$ denotes the rate of blood flow out of the compartment. Note that Eq [2] is simply a conservation of mass equation for deoxyhemoglobin. Changes in blood volume are governed by two differential equations. The first equation (Eq [3]) determines the rate of change of $v(t)$ given the difference between the current value of $v(t)$ and the value that $v(t)$ would reach if the system were allowed to reach a steady state ($f_{in}\alpha v$) where α_v is the exponential flow-volume coupling parameter as described by Grubb et al., though in this model its value is not fixed (Grubb et al., 1974):

$$dv/dt = (1/\tau_v) \times (f_{in}^{av}(t) - v(t)) \quad (3)$$

The second equation (Eq [4]) is simply a conservation rule for blood volume that determines the flow out of the system, $f_{out}(t,v)$, given the inflow and volume change:

$$dv/dt = (1/\tau_0) \times (f_{in}(t) - f_{out}(t,v)) \quad (4)$$

To describe $f_{in}(t)$ and $r(t)$, we assumed that each response could be described as a linear response to the instantaneous stimulus contrast $c(t)$:

$$f_{in}(t) = c(t) * h_f(t) \quad (5)$$

$$r(t) = c(t) * h_r(t) \quad (6)$$

where the convolution kernel $h(t)$ is a scaled gamma distribution,

$$h_{f,r} = H_{f,r} \times t^{(z-1)} \times e^{(-t/\tau,f,r)}/(\tau_{f,r})^z/(Z-1)! \quad (7)$$

where $x_{f,r}$ denotes that each parameter in the model has a unique value to describe the CBF or CMRO$_2$ response.

In order to minimize the number of unmeasured parameters in the model, we did not explicitly account for the effects of intravascular signal decay on the BOLD response. Under these conditions, the BOLD signal change produced by a change in deoxyhemoglobin content may be approximated by the equation (Obata et al., 2004)

$$(b(t) - b_0)/b_0 \approx -\Delta R_2^*(t) \times TE = -\psi \times (q(t) - 1) \times TE$$

where $\psi = 4.3\nu_0 V_0 E_0 \approx 3$ for a magnetic field strength of 3T, assuming the frequency offset produced by a fully deoxygenated blood vessel, $\nu_0 = 80.6s-1$ (Obata et al., 2004)a baseline fractional CBV$_v$, $V_0 = 0.02$, and baseline oxygen extraction fraction, $E_0 = 0.4$ (Leenders et al., 1990). In ignoring the effects of intravascular signal decay, we are likely to underestimate the BOLD signal change associated with a given $q(t)$ and ψ, the latter of which acts like a scaling parameter (much like A in Equation 1). However, as we will show, the results of our analysis are not dependent on the precise value of ψ, and are thus unlikely to be strongly affected by this simplification of the model.

2.2 Simulating experimental measurements of BOLD and CBF

In the experimental portion of this work, we measured the BOLD and CBF responses to visual stimuli using a QUIPSS-II pulsed ASL imaging sequence with a dual echo spiral readout (Wong et al., 1998). In this sequence, the magnetization of arterial blood is inverted or not inverted ("tag" or "control") on alternating samples, proximal to the imaging slice. Blood is allowed to flow out of the tagging region for a period of time denoted TI1. At t=TI1, a saturation pulse is applied to the tagging region. At t=TI2, an excitation pulse is applied to the imaging plane and images are acquired with the dual-echo spiral readout. To minimize R$_2$* weighting, the images used for CBF estimation are acquired with a very short echo time (here 3.3ms). Because the signal of the static tissue in the imaging plane is

unaffected by the tag/control labeling scheme, the difference signal between tag and control images is proportional to the amount of labeled arterial blood delivered to the imaging volume between the tag and excitation pulses. This difference signal may be constructed by modulation and temporal low-pass filtering of the measured signal and used to estimate CBF (Liu and Wong, 2005). To maximize R_2^* weighting, the images used for BOLD estimation are acquired at the second, later echo time (here 30ms). BOLD-weighted images are then constructed by temporal low-pass filtering (without modulation) of the image series.

Due to this image acquisition procedure, the measured CBF-weighted signal (in the absence of noise), is a low pass filtered representation of the *average* blood flow between inversion and excitation pulses while the measured BOLD-weighted signal is a low pass filtered representation of the instantaneous BOLD signal at the time of the excitation pulse. To account for these discrepancies between ideal and measured time series, simulated CBF and BOLD time series were generated with a much higher sampling rate than the measured time series ($10s^{-1}$ vs. $0.5s^{-1}$). The simulated CBF time series were then averaged over the time period corresponding to the time between inversion and excitation at each sample. This averaging procedure produced a down-sampled version of the CBF time course with the same temporal resolution as the measured data. This down-sampled time course was then low-pass filtered with the same filter used to produce the measured CBF time series (see Section 3.4 for details). The simulated BOLD time series were simply down-sampled to match the measured BOLD time series and then low-pass filtered.

3. Methods

3.1 Subjects

Ten healthy adult subjects participated in this study (7 male, mean age 29, range 25-33 years). The studies were approved by the institutional review board at the University of California San Diego and written informed consent was obtained from all participants.

3.2 Imaging

Simultaneous BOLD and CBF-weighed images were acquired on a GE Discovery 740 3T scanner with a dual-echo arterial spin labeling (ASL) PICORE QUIPSS II sequence (Wong et al., 1998) with a spiral readout. ASL sequence parameters were 4 slices (5mm thick/1mm gap) covering the calcarine sulcus, TR 2.0s, TI1/TI2 700/1700ms, TE1 3.3ms, TE2 30ms, 90° flip angle, FOV 240mm, and matrix 64x64. A field map was additionally acquired for use in correcting distortions in the spiral images due to the inhomogeneity of the magnetic field (Noll et al., 2005). Throughout each scan cardiac and respiratory activity were recorded using a pulse oximeter and respiratory bellows.

3.3 Stimulus Paradigm

Visual Stimuli were produced using MATLAB® (2009a, The MathWorks, Natick, MA) with the Psychophysics Toolbox extensions (Pelli, 1997). The stimulus consisted of a gray scale flickering radial checkerboard with a central region (visual angle ~1.5°) that was maintained an iso-luminescent gray. The dark-light reversal frequency was 8Hz and the dark-light contrast could be adjusted from 0% (uniform gray) to 100% (black and white) in

increments of 1%. The visual stimulus was projected onto a screen, which the subject could view through a head coil mounted mirror.

Each study consisted of five functional (task) runs during which BOLD and CBF-weighted images were acquired. Throughout each of the functional tasks, the subjects were asked to fixate on the center of the screen. In order to maintain the subjects' attention, random numbers (0-9) were displayed in the gray central region of the screen at 1s intervals. The subjects were instructed to press a button on a response box each time a number was displayed twice in a row. The first functional run was used to locate a region of interest (ROI) in the visual cortex. The stimulus paradigm consisted of 24s of 0% contrast followed by 6 cycles during which the stimulus contrast alternated between 100% and 0% at 24s intervals. The other four functional runs were used for quantitative analysis. Each of these runs consisted of 68s of 0% contrast followed by 308s during which the contrast oscillated in a sinusoidal manner from 0% to 100% with a period of 44s, 22s, 11s, or $44/7 \approx 6.3$s. During the final 30s of each run the contrast was again maintained at 0%. The order in which each of the four stimulus periods were presented was changed for each subject so as to minimize any bias due to fatigue.

3.4 Preprocessing

Raw images were first corrected for distortions due to the inhomogeneity of the magnetic field (Noll et al., 2005). The first four images of each scan were discarded to allow the MRI signal to reach steady state. All functional runs were motion corrected and registered to the first functional run using AFNI software (Cox, 1996). In order to produce a CBF-weighted image series, the 4-D, first-echo data set was first temporally modulated at a frequency of 0.25Hz (i.e. ASL "tag" images were multiplied by –1) and then temporally low-pass filtered (Liu and Wong, 2005). In order to minimize the attenuation of the response to the 11s stimulus, the low pass filter was designed to have a passband from 0-0.09Hz and a stopband from 0.16-0.25Hz. The MATLAB® function *firpm* was used to generate a finite impulse response filter with these characteristics. To produce a BOLD-weighted image series, the 4-D second-echo data set was temporally filtered using this same low-pass filter but without prior modulation.

Statistical analysis for ROI selection was performed on the first functional run using a general linear model (GLM) approach for the analysis of ASL data as we have previously described (Perthen et al., 2008). Briefly, a stimulus regressor was produced by convolving the stimulus pattern with a gamma density function (Boynton et al., 1996). Cardiac and respiratory signals were used as regressors to account for the non-stimulus related signal variance produced by physiological processes (Glover et al., 2000; Restom et al., 2006). A constant and a linear term were also included as regressors. An anatomical mask that included only gray matter voxels in the posterior half of the brain was produced for each subject, and ROI selection was restricted to this region. Voxels exhibiting CBF or BOLD activation were detected after correcting for multiple comparisons using AFNI AlphaSim (Cox, 1996), using an overall significance threshold of p = 0.05 given a minimum cluster size of four voxels. For each subject, an active visual cortex region of interest (ROI) was defined as those voxels exhibiting both CBF and BOLD activation independently.

Activation detection analysis was not performed on the four contrast-oscillating runs. In addition, we chose not to correct these runs for physiological noise or signal drifts before quantitative analysis. Linear drift correction was not implemented because the stimulus paradigm was not temporally symmetrical with respect to the midpoint of the experiment, producing a real non-zero correlation between the time courses and a linear regressor that if removed would quantitatively bias our data. Cardiac and respiratory activity-derived regressors were not used to remove physiological noise from the time series as a conservative measure given the lack of literature evidence that doing so does not quantitatively bias the resulting BOLD and CBF activations.

3.5 Comparison of Measured CBF and BOLD responses to the dynamic model

Before fitting the model parameters to the measured data, the 4-D BOLD and CBF image series from each subject were first averaged over the ROI defined for that subject to produce 1-D BOLD and CBF time series. These time series were then normalized with respect to their mean baseline values, defined as the 60s before the stimulus began, and averaged across subjects, producing a single pair of BOLD and CBF time series for each stimulus frequency.

The parameters defining the dynamic model were simultaneously fit to the subject-averaged BOLD and CBF time series across all stimulus frequencies using the MATLAB function *fmincon* (2011a, The MathWorks, Natick, MA). We found that the fit would not converge if all of the parameters of the model were allowed to be free and as such decided to fix the values of several of the parameters based on previous reports from the literature while allowing the key parameters controlling the amplitude and dynamics of the CBF, $CMRO_2$, and CBV_v responses to be fit to the data. We then varied the fixed parameters and repeated the fitting process to determine if our conclusions about the relative dynamics of CBF, $CMRO_2$, and CBV_v were sensitive to the values of these parameters. The fixed parameters in the model were the BOLD-deoxyhemoglobin scaling parameter, $\psi=3$ (see references in Section 2.2), the vessel transit time, $\tau_0=2s$ (Obata et al., 2004), and the shape parameter in the impulse response function, $z=3$ (Boynton et al., 1996). The free parameters of the model were the CBF, $CMRO_2$, and CBV_v response amplitudes (H_f, H_r, and α_v, respectively) and time constants (τ_f, τ_r, and τ_v, respectively).

4. Results

4.1 Predicting the effect of dynamic decoupling on the BOLD and CBF responses to oscillating stimulation

Before fitting the dynamic model to the measured data set, we simulated the relationship between BOLD and CBF responses to sinusoidal contrast oscillation that would be expected given the dynamic decoupling necessary to produce the most commonly observed BOLD signal transients, namely the 'initial dip' and the 'post-stimulus undershoot'. The simulations are not intended to represent an exhaustive set of potential dynamics but to illustrate the range of effects that dynamic decoupling could have on the BOLD-CBF relationship. Figure 1 shows simulated CBF, $CMRO_2$, and CBV_v responses that produce these BOLD transients in response to a standard 20s boxcar stimulus as well as the

relationship between CBF and BOLD fluctuations that would result from continuous stimulation with the contrast oscillating stimuli used in this experiment. The top row (a-c) depicts responses to boxcar and sinusoidal stimuli assuming tight coupling of CBF, $CMRO_2$, and CBV_v dynamics ($\tau_r = 2s$, $\tau_f = 2s$, $\tau_v = 0s$). Tight dynamic coupling produces no transients in the BOLD response to a boxcar stimulus. Similarly, the relationship between BOLD and CBF fluctuations in response to the sinusoidal stimulus is well described by a discrete-time signal extension of Equation 1 in the case where n and α_v are fixed (depicted by black-dotted line in Figure 1c). The small amount of hysteresis in the BOLD-CBF relationship is due to the finite transit time ($\tau_0 = 2s$) for blood passing through the vascular compartment and to the sensitivity of the ASL measurement to the average blood flow over the period between inversion and excitation. These two processes have opposite effects on the BOLD-CBF relationship and cancel (meaning hysteresis disappears) for $\tau_0 = 1s$. The middle row (d-f) depicts responses to boxcar and sinusoidal stimuli assuming faster dynamics in the $CMRO_2$ response than CBF or CBV_v ($\tau_r = 1.5s$, $\tau_f = 2s$, $\tau_v = 0s$). This produces an 'initial dip' (Figure 1e) in the BOLD response to a boxcar stimulus. In response to the sinusoidal stimulus, the more rapid $CMRO_2$ dynamics are predicted to produce significant hysteresis in the BOLD-CBF relationship that becomes increasingly pronounced as the oscillation period decreases (Figure 1f). The bottom row (g-i) depicts responses to boxcar and sinusoidal stimuli assuming much slower dynamics in the CBV_v response than CBF or $CMRO_2$ ($\tau_r = 2s$, $\tau_f = 2s$, $\tau_v = 20s$), producing a 'post-stimulus undershoot' in the BOLD response to the boxcar stimulus (Figure 1h). In response to the sinusoidal stimulus, the slow CBV_v dynamics are predicted to produce a shift rather than hysteresis in the BOLD-CBF relationship that is independent of the period of contrast oscillation (Figure 1i). Note that the trajectories depicted in Figure 1i reflect the relationship between BOLD and CBF fluctuations after a prolonged period of stimulation, meaning that CBV_v has had the opportunity to slowly rise in response to the envelope of the stimulus to an approximately steady state.

4.2 Measured CBF and BOLD responses to continuously modulated stimulation

At each frequency tested, the visual stimulus evoked a robust response in both CBF and the BOLD signal (Figure 2). In general this response was characterized by a significant increase in the mean BOLD and CBF signals that corresponded with the envelope of the stimulus and was modulated at the frequency of the contrast oscillations. An interesting feature of these time courses is a clear decay in the magnitudes of the envelopes of the BOLD responses to the 22s, 11s, and 6.3s stimuli over approximately the first 40s of stimulation, a pattern that, if present in the CBF responses, is significantly less pronounced. Similarly, in response to the 44s stimulus, the BOLD signal troughs dip well below baseline, while the CBF troughs do not. It may also be noted that there are no periodic oscillations in the BOLD and CBF responses to the 6.3s period stimulus. This is because the frequency of stimulus oscillation ($\sim0.16s^{-1}$) is higher than the Nyquist frequency for an ASL experiment with a TR of 2s (Nyquist frequency for ASL is ¼ of the sampling frequency due to tag-control imaging). This frequency was chosen so that we could look for a characteristic aliasing artifact reflecting BOLD contamination of the CBF signal that, if significant, would be observable as a periodic, $1/11s^{-1}$ oscillation in the CBF response. Such an oscillation was not observed,

but this data set was included in the analysis because it still contained the lower frequency components of the CBF and BOLD responses.

Figure 3 displays the average BOLD (3a) and CBF (3b) responses to each stimulus over one contrast-oscillation cycle, as well as the relationship between the average BOLD and CBF responses (3c). The averages exclude the first 44s seconds of the stimulus period (equivalent to the first cycle of the lowest frequency stimulus) such that all included time points reflect recovery from a previous cycle. That is, the plotted trajectories reflect dynamics during the sustained response, excluding the initial stimulus onset response, and the BOLD and CBF responses are expressed as fractions of the baseline data before the stimulus began. The BOLD-CBF trajectories shown in Figure 3c show little evidence of the hysteresis pattern that characterized the BOLD-CBF relationship in Figure 1f, suggesting that the dynamics of the $CMRO_2$ response are not likely to be significantly faster than those of the CBF response. However, the trajectories in Figure 3c do show evidence of a shift, such that as CBF returns to baseline, the BOLD signal dips significantly below baseline. This pattern is similar to that depicted in Figure 1i, which simulates the BOLD-CBF trajectory when the dynamics of the CBV_v response are an order of magnitude slower than those of CBF and $CMRO_2$.

4.3 Comparison of Measured CBF and BOLD responses to the dynamic model

To test how well the observed slow decay in the BOLD signal and shift in the BOLD-CBF response trajectories could be explained by a slow CBV_v or $CMRO_2$ response to the stimulus, we fit the CBF, $CMRO_2$, and CBV_v response amplitudes (H_f, H_r, and a_v, respectively) and time constants (τ_f, τ_r, and τ_v, respectively) in the dynamic model to the measured data, assuming $\psi=3$, $\tau_0=2s$, and $z=3$. We found that the model fit equally well to the data if either the CBV_v or $CMRO_2$ response was an order of magnitude slower than the CBF response. The best-fit set of parameters for the slow CBV_v response was $\tau_r=2.3s$, τ_v $=27.5s$, $\tau_f=2.1s$, $H_r=0.26$, $a_v=0.28$, $H_f=0.82$, while for the slow $CMRO_2$ response it was $\tau_r=13.6s$, $\tau_v=3.3s$, $\tau_f=2.1s$, $H_r=0.13$, $a_v=0.46$, $H_f=0.82$. If τ_0 was assumed to be less than 0.75s or greater than 2.5s, a slow $CMRO_2$ response would not provide a robust fit to the data. Varying the value of τ_0 had a small quantitative effect on the best-fit values of τ_r and τ_v (both decreased with decreasing τ_0), however, it did not change the qualitative picture that either τ_r or τ_v had to be much greater than τ_f. Increasing the assumed value of ψ to a value as high as 7 was compatible with either a slow CBV_v or $CMRO_2$ response. Increasing the value of ψ had little effect on the dynamics of the $CMRO_2$ and CBV_v responses; however, it did have a large effect on the best-fit values of H_r and a_v, generally increasing the magnitude of the rapidly responding process and decreasing the magnitude of the slowly responding process. If the assumed value of ψ was decreased to 2, then $\tau_r=12.9$, $\tau_v=9.0$, H_r $=0.21$, $a_v=0.14$ was the unique, best-fit solution, meaning that both the CBV_v and $CMRO_2$ responses would have to be an order of magnitude slower than CBF. Varying the assumed value of the gamma impulse shape parameter, z, within the range of 2-4 did not qualitatively affect our conclusions about the relative dynamics of CBF, $CMRO_2$, and CBV_v.

Because of the quantitative sensitivity of the model parameter estimates to the assumed values of ψ, τ_0, and z, we cannot make quantitative claims about the dynamics of the individual CBF, $CMRO_2$, or CBV_v responses from this data set alone, nor can we make

precise quantitative claims about the magnitudes of the $CMRO_2$ and CBV_v responses. However, analysis of the measured responses with the dynamic model does suggest that either $CMRO_2$ or CBV_v responds on a timescale that is an order of magnitude slower than CBF. Figure 4 displays the measured BOLD and CBF responses to each stimulus as well as the simulated responses for $\tau_r = 2.3s$, $\tau_v = 27.5s$, $\tau_f = 2.1s$, $H_r = 0.26$, $a_v = 0.28$, $H_f = 0.82$, $\psi = 3$, $\tau_0 = 2s$, and $z = 3$ (slow CBV_v response). Note that while the model does not perfectly replicate all of the features of the BOLD and CBF responses to the stimulus (most notably that the trough-to-peak and peak-to-trough times are not equal in the measured BOLD and CBF responses to the 44s and 22s stimuli, likely due to a non-linearity in the CBF and $CMRO_2$ responses to the stimulus itself), it does nicely replicate the most salient features of the measured responses, namely the amplitudes and phases of the CBF and BOLD oscillations for each stimulus, as well as the slow decay of the BOLD signal. The simulated responses corresponding to the slow $CMRO_2$ response are not visually distinguishable from those shown in Figure 4 and so are not shown here.

Based upon our ability to fit the measured data set, either the slow CBV_v or $CMRO_2$ response hypothesis is equally plausible. However, based on the relative magnitudes of the $CMRO_2$ and CBV_v responses implied by each hypothesis, we believe our findings are more consistent with a slow CBV_v response. Figure 5 displays the CBF, $CMRO_2$, and CBV_v responses associated with slow CBV_v dynamics (top row) or slow $CMRO_2$ dynamics (bottom row), over a single stimulus cycle, after a prolonged period of stimulation. While the precise magnitudes of the $CMRO_2$ and CBV_v responses depend upon the assumed value of ψ, the relative magnitudes of these responses do not. For the slow CBV_v case, the $CMRO_2$ response is of a greater magnitude than the CBV_v response, while the reverse is true of the slow $CMRO_2$ case. Figure 5d and 5h show the responses to the 6.3s stimulus, which do not fluctuate appreciably over a stimulus cycle but do reflect the mean response to the stimulus. For the slow CBV_v response, CBF increases by 41%, while the predicted $CMRO_2$ increases by 13% and the predicted CBV_v increases by 9.5%. This makes the ratio of the CBF to the $CMRO_2$ response approximately 3, which is within range (typically 2-4) of previous reports (Buxton, 2010). Similarly, the ratio of the CBF response to CBV_v response is approximately 4, consistent with the most recent quantitative measurements of the CBV_v response (Chen and Pike, 2009b). Conversely, for the slow $CMRO_2$ response, the predicted $CMRO_2$ increases only 6.2% while the predicted CBV_v increases 16.5%, bringing the ratio of the CBF to $CMRO_2$ response to approximately 6 and the CBF to CBV_v response to 2.5. While CBF-$CMRO_2$ ratios as high as 6 have been reported (Fox and Raichle, 1986), the CBV_v change is considerably larger than what is typically reported. Increasing the assumed value of ψ (to account for intravascular effects) only decreases the predicted $CMRO_2$ response and increases the predicted CBV_v response in the slow $CMRO_2$ dynamics case. For $\psi = 5$, the predicted $CMRO_2$ response to the 6.3s stimulus is only 3.6% while the predicted CBV_v response is 26%.

5. Discussion

The BOLD signal is currently the leading approach for mapping dynamic patterns of activity in the human brain. Due to the physiological complexity of the signal, however, it is not possible to interpret the BOLD signal as a quantitative reflection of the magnitude of the

underlying neural activity, or even the underlying physiological changes in CBF and CMRO$_2$. The calibrated BOLD approach has the potential to address the quantitative limitations of BOLD imaging, and in a number of simple experiments, has demonstrated sensitivity to subtleties in the physiological response to neural stimulation that lead to incorrect conclusions when observed through BOLD imaging alone (Ances et al., 2008; Griffeth et al., 2011; Liang et al., 2013). As interest is shifting from using BOLD imaging to map brain regions that respond to simple stimuli to analyzing the complex spatial and temporal characteristics of BOLD signals during unconstrained experiments (Smith et al., 2009; Snyder and Raichle, 2012), it would be useful to be able to employ quantitative imaging techniques under more dynamic conditions. While the interpretation of simple block design experiments can be based just on the steady-state relationships between CBF, CMRO$_2$, and CBV$_v$, the extension of current quantitative methods, such as calibrated BOLD, to dynamic experimental conditions depends upon dynamic coupling of the physiological variables that underlie the BOLD phenomenon (Herman et al., 2009).

In this study we looked for evidence of dynamic decoupling of the CBF, CMRO$_2$, and CBV$_v$ responses in the human brain to visual stimuli that oscillated in contrast at several temporal frequencies, using a dynamic model of the BOLD response to infer the relative dynamics of the CBF, CMRO$_2$, and CBV$_v$ responses from measured CBF and BOLD responses. We found that the measured CBF and BOLD responses were best explained by close coupling of the CBF and CMRO$_2$ responses to contrast oscillation and a CBV$_v$ response that was an order of magnitude slower to develop than either CBF or CMRO$_2$. This slow CBV$_v$ response would produce a slow decay in the envelope of the BOLD response to a continuously oscillating stimulus independently of the frequency of contrast oscillation, as was observed in this study, and cause the relationship between CBF and BOLD fluctuations to shift away from the relationship predicted by a model of the BOLD response (Equation 1) that assumed close coupling of CBF, CMRO$_2$, and CBV$_v$. Our model suggested that this phenomenon could be equally well explained if the dynamics of the CMRO$_2$ response, rather than those of the CBV$_v$ response, were an order of magnitude slower than those of CBF; however, we concluded that a slow CBV$_v$ response was more plausible, as a slow CMRO$_2$ response would require the magnitude of the CBV$_v$ response to be significantly larger than what has been reported in the literature (Chen and Pike, 2009b).

5.1 Dynamics of CBF, CMRO$_2$ and CBV$_v$ responses to neural stimuli

Previous reports of CBV$_v$ dynamics are generally consistent with the idea that the CBV$_v$ response is considerably slower than that of CBF. For example, In the rat sensory cortex, Hillman and colleagues found no change in venous vessel diameter in response to a 4s forepaw stimulus, in spite of a robust change in arteriolar diameter (Hillman et al., 2007). Similarly, in the mouse vibrissa cortex, Drew and colleagues found that arterial but not venous diameter responded to punctate whisker stimulation, and that in response to prolonged stimulation, venous diameter increased with a time constant of approximately 40s (Drew et al., 2011). In the cat visual cortex, Kim and Kim measured changes in arterial CBV and total CBV in response to a 40s visual stimulus using MOTIVE and MION-contrast MRI, respectively, finding that the difference in the two responses was consistent with a CBV$_v$ response with a time constant of 20-40s (T. Kim and S.-G. Kim, 2010). Finally, in a

human study employing VERVE MRI to directly measure CBV_v, Chen and Pike found that CBV_v returned to baseline significantly more slowly than CBF after stimulus cessation (Chen and Pike, 2009a).

In contrast, previous reports of the dynamics of $CMRO_2$ generally suggest that the $CMRO_2$ response to neural stimulation is more rapid than that of CBF (Devor et al., 2005; Malonek and Grinvald, 1996). While several studies in *ex vivo* systems have suggested that oxidative metabolism remains elevated for minutes after stimulation has ceased (Hall et al., 2012; Kasischke, 2004), Vazquez et al. found in an *in vivo* rat model that mitochondrial oxidative metabolism responded within seconds to both the onset and offset of neural stimulation (Vazquez et al., 2012). Similarly, while a number of MRI-based studies in humans have found that total CBV returns to baseline significantly before the end of the BOLD post stimulus undershoot, which some have interpreted as evidence of continued post-stimulus metabolic activity (Donahue et al., 2009; Frahm et al., 2008; Lu et al., 2004), studies looking more specifically at venous CBV have found much slower returns to baseline, suggesting that total CBV measurements may be dominated by arterial contributions and should be interpreted with caution (Chen and Pike, 2009a; T. Kim and S.-G. Kim, 2010).

Interestingly, Hoge et al. observed BOLD signal decay that was similar to the decay observed in this study in response to sustained (7 min) stimulation with a flickering checkerboard whose contrast did not vary. In addition, they observed a significant decay in a simultaneously measured perfusion signal and attributed their findings to transient activation of a subset of neurons with high contrast sensitivity (Hoge et al., 1999). It is unclear whether there is a relationship between Hoge's findings and our own, as the contrast of our stimulus oscillated continuously while Hoge's remained constant over the stimulus period. However, the potential for an underlying role for neural and/or hemodynamic adaptation in producing BOLD transients such as those observed in this study is intriguing and merits future investigation.

It similarly merits noting that in a recent investigation into the effect of image contrast on the CBF-$CMRO_2$ coupling ratio, *n*, our group found statistically significant differences in the coupling ratios estimated from the BOLD and CBF responses to low and high contrast stimuli, with high contrast stimuli evoking both larger BOLD and CBF responses as well as higher coupling ratios (Liang et al., 2013). This phenomenon has the potential to produce an effect on the CBF-BOLD relationship similar to the one observed in this study, wherein the trajectory of the CBF-BOLD relationship is less concave than predicted by Equation 1. It is likely that this effect had some influence on the shape of the CBF-BOLD relationship observed in this study, though it is challenging to estimate its magnitude both due to differences in study design (e.g. in the previous study each measurement corresponded to a single stimulus contrast presented in block design fashion, while in this study contrast varied continuously) and because calibration data was not available for either study. However, this effect cannot fully explain the observed slow decay in the BOLD response envelope nor the deep negative signal troughs in BOLD response to the 44s stimulus observed here, as, in the Liang study, even a stimulus with 1% contrast evoked a robust and positive BOLD response. We believe these findings are more easily explained by a CBV_v (or $CMRO_2$) that remained elevated even as CBF returned toward baseline between stimulus cycles.

5.2 Implications of slow CBV_v response for dynamic quantitative fMRI

The decoupling of CBV_v and CBF dynamics inferred in this study presents a potential challenge for the extension of quantitative fMRI techniques such as calibrated BOLD to the study of dynamically fluctuating neural activity. As discussed above, because all of the physiological inputs to the BOLD signal cannot currently be measured simultaneously in an fMRI experiment, direct extension of current techniques requires the assumption that there are few degrees of freedom between fluctuations in CBF and the BOLD signal. This assumption can lead to inaccurate estimates of the metabolic response if the system has not reached a steady state. For example, if the flow-volume coupling constant (α_v) in Equation 1 were assumed to be constant and equal to 0.2 (Chen and Pike, 2009b), then for A=0.1, δb = 0.01, δf = 0.4, the estimated change in $CMRO_2$ would be approximately 18%. However, if volume changes were assumed to lag behind flow changes, such that early in the stimulus period α_v were effectively near zero, then the estimated change in $CMRO_2$ would be approximately 26% at this time, a relative discrepancy of approximately 45%. The difficulty of dynamic $CMRO_2$ estimation is compounded by the low signal-to-noise ratio of the ASL CBF signal, which makes sample-to-sample estimation of CBF challenging; however, a conservative interpretation of our findings would be that, at a minimum, simultaneous measurement of CBV_v, CBF, and BOLD is necessary for highly accurate dynamic estimation of $CMRO_2$ fluctuations associated with neural activity. Unfortunately, there is currently no simple way to measure venous CBV distinctly from total CBV, although hyperoxia is a promising approach (Blockley et al., 2012).

The idea that α_v is not time-invariant also has implications for more traditional analyses with block-design stimuli, as it suggests that the value of α_v is likely to be highly dependent upon the length of the stimulus block and the time period within which BOLD and CBF measurements are averaged in order to estimate the $CMRO_2$ response. The findings of this work would suggest that a relatively long period of time (~40s) might be required for CBV_v to achieve a steady state response to a constant stimulus, over which time the effects of neural adaptation could become significant (Moradi and Buxton, 2013). For researchers who need to use shorter stimulus blocks, an analysis of the sensitivity of their findings to the possibility that α_v may be significantly smaller than what is reported in the literature might be appropriate.

An important question moving forward is how much effect CBV_v has on the BOLD signal and dynamic $CMRO_2$ estimation over the frequency spectrum of interest in a naturalistic stimuli fMRI experiment, which may extend from 0.001 to 0.2Hz (Niazy et al., 2011). Based on the results of this study, we predict that the CBV_v changes associated with CBF and BOLD fluctuations at frequencies >0.02Hz are essentially negligible and may be ignored without significantly affecting associated $CMRO_2$ estimates. This likely explains our early success in using BOLD constrained perfusion (BCP), a technique that estimates CBF-$CMRO_2$ coupling from BOLD-ASL time series without requiring knowledge of the stimulus pattern but requires the assumption of tight dynamic CBF-$CMRO_2$-CBV_v coupling, to estimate the coupling ratio (*n*) associated with a stimulus consisting of intermittent, short (20s) stimulus blocks (Simon et al., 2013). However, the results of this study also suggest that techniques such as BCP may not perform as well with time series containing significant

low frequency components, where the effects of CBV_v decoupling are more prominent. A full analysis of the impact of this decoupling on the BCP approach is beyond the scope of this work. However, such an analysis, in part using the empirical data reported here, will be presented in a subsequent report.

5.5 Conclusions

Quantitative fMRI techniques designed to measure the hemodynamic and metabolic responses to neural activity have demonstrated sensitivity to aspects of the physiological response to neural activity that cannot be captured by BOLD imaging alone. However, their applicability to the study of natural behavior and cognition is limited by our current inability to simultaneously capture the dynamics of all of the physiological inputs to the BOLD signal. In this study we looked for evidence of dynamic decoupling in these physiological inputs, finding evidence consistent with a relatively closely coupled metabolic and blood flow response and a much slower venous blood volume response. These findings suggest that for studies of brain dynamics, that do not involve large sustained changes in CBF, the slow changes in venous CBV are likely to be a small effect in determining the dynamics of metabolism. In general, though, for large sustained changes comparable to those in the current study, the effect of venous blood volume fluctuations may be required for precise estimation of dynamic metabolic fluctuations.

Acknowledgements

References

Ances BM. Coupling of Changes in Cerebral Blood Flow with Neural Activity: What Must Initially Dip Must Come Back Up. Journal of Cerebral Blood Flow & Metabolism. 2004:1–6. doi: 10.1097/01.WCB.0000103920.96801.12. [PubMed: 14688611]

Ances BM, Leontiev O, Perthen JE, Liang C, Lansing AE, Buxton RB. Regional differences in the coupling of cerebral blood flow and oxygen metabolism changes in response to activation: Implications for BOLD-fMRI. NeuroImage. 2008; 39:1510–1521. doi:10.1016/j.neuroimage. 2007.11.015. [PubMed: 18164629]

Attwell D, Laughlin SB. An energy budget for signaling in the grey matter of the brain. Journal of Cerebral Blood Flow & Metabolism. 2001; 21:1133–1145. doi: 10.1097/00004647-200110000-00001. [PubMed: 11598490]

Blockley NP, Driver ID, Fisher JA, Francis ST, Gowland PA. Measuring venous blood volume changes during activation using hyperoxia. NeuroImage. 2012; 59:3266–3274. doi:10.1016/j.neuroimage.2011.11.041. [PubMed: 22146751]

Boynton GM, Engel SA, Glover GH, Heeger DJ. Linear systems analysis of functional magnetic resonance imaging in human V1. J. Neurosci. 1996; 16:4207–4221. [PubMed: 8753882]

Buxton RB. Interpreting oxygenation-based neuroimaging signals: the importance and the challenge of understanding brain oxygen metabolism. Front. Neuroenerg. 2010 doi:10.3389/fnene.2010.00008.

Buxton RB. The physics of functional magnetic resonance imaging (fMRI). Rep. Prog. Phys. 2013; 76:096601. doi:10.1088/0034-4885/76/9/096601. [PubMed: 24006360]

Buxton RB, Wong EC, Frank LR. Dynamics of blood flow and oxygenation changes during brain activation: the balloon model. Magn. Reson. Med. 1998; 39:855–864. [PubMed: 9621908]

Chen JJ, Pike GB. Origins of the BOLD post-stimulus undershoot. NeuroImage. 2009a; 46:559–568. doi:10.1016/j.neuroimage.2009.03.015. [PubMed: 19303450]

Chen JJ, Pike GB. BOLD-specific cerebral blood volume and blood flow changes during neuronal activation in humans. NMR Biomed n/a–n/a. 2009b doi:10.1002/nbm.1411.

Cox RW. AFNI: software for analysis and visualization of functional magnetic resonance neuroimages. Comput. Biomed. Res. 1996; 29:162–173. [PubMed: 8812068]

Davis TL, Kwong KK, Weisskoff RM, Rosen BR. Calibrated functional MRI: mapping the dynamics of oxidative metabolism. Proc. Natl. Acad. Sci. U.S.A. 1998; 95:1834–1839. [PubMed: 9465103]

Devor A, Ulbert I, Dunn AK, Narayanan SN, Jones SR, Andermann ML, Boas DA, Dale AM. Coupling of the cortical hemodynamic response to cortical and thalamic neuronal activity. Proc. Natl. Acad. Sci. U.S.A. 2005; 102:3822–3827. doi:10.1073/pnas.0407789102. [PubMed: 15734797]

Donahue MJ, Blicher JU, Østergaard L, Feinberg DA, MacIntosh BJ, Miller KL, Günther M, Jezzard P. Cerebral blood flow, blood volume, and oxygen metabolism dynamics in human visual and motor cortex as measured by whole- brain multi-modal magnetic resonance imaging. Journal of Cerebral Blood Flow & Metabolism. 2009; 29:1856–1866. doi:10.1038/jcbfm.2009.107. [PubMed: 19654592]

Drew PJ, Shih AY, Kleinfeld D. Fluctuating and sensory-induced vasodynamics in rodent cortex extend arteriole capacity. Proc. Natl. Acad. Sci. U.S.A. 2011; 108:8473–8478. doi:10.1073/pnas. 1100428108. [PubMed: 21536897]

Fox PT, Raichle ME. Focal physiological uncoupling of cerebral blood flow and oxidative metabolism during somatosensory stimulation in human subjects. Proc. Natl. Acad. Sci. U.S.A. 1986; 83:1140–1144. [PubMed: 3485282]

Frahm J, Baudewig J, Kallenberg K, Kastrup A, Merboldt KD, Dechent P. The post-stimulation undershoot in BOLD fMRI of human brain is not caused by elevated cerebral blood volume. NeuroImage. 2008; 40:473–481. doi:10.1016/j.neuroimage.2007.12.005. [PubMed: 18201912]

Glover GH, Li TQ, Ress D. Image-based method for retrospective correction of physiological motion effects in fMRI: RETROICOR. Magn. Reson. Med. 2000; 44:162–167. [PubMed: 10893535]

Griffeth VEM, Blockley NP, Simon AB, Buxton RB. A New Functional MRI Approach for Investigating Modulations of Brain Oxygen Metabolism. PLoS ONE. 2013; 8:e68122. doi: 10.1371/journal.pone.0068122. [PubMed: 23826367]

Griffeth VEM, Buxton RB. A theoretical framework for estimating cerebral oxygen metabolism changes using the calibrated-BOLD method: Modeling the effects of blood volume distribution, hematocrit, oxygen extraction fraction, and tissue signal properties on the BOLD signal. NeuroImage. 2011; 58:198–212. doi:10.1016/j.neuroimage.2011.05.077. [PubMed: 21669292]

Griffeth VEM, Perthen JE, Buxton RB. Prospects for quantitative fMRI: investigating the effects of caffeine on baseline oxygen metabolism and the response to a visual stimulus in humans. NeuroImage. 2011; 57:809–816. doi:10.1016/j.neuroimage.2011.04.064. [PubMed: 21586328]

Grubb RL, Raichle ME, Eichling JO, Ter-Pogossian MM. The effects of changes in $PaCO_2$ on cerebral blood volume, blood flow, and vascular mean transit time. Stroke. 1974; 5:630–639. [PubMed: 4472361]

Hadjikhani N, Sanchez Del Rio M, Wu O, Schwartz D, Bakker D, Fischl B, Kwong KK, Cutrer FM, Rosen BR, Tootell RB, Sorensen AG, Moskowitz MA. Mechanisms of migraine aura revealed by functional MRI in human visual cortex. Proc. Natl. Acad. Sci. U.S.A. 2001; 98:4687–4692. doi: 10.1073/pnas.071582498. [PubMed: 11287655]

Hall CN, Klein-Flugge MC, Howarth C, Attwell D. Oxidative Phosphorylation, Not Glycolysis, Powers Presynaptic and Postsynaptic Mechanisms Underlying Brain Information Processing. Journal of Neuroscience. 2012; 32:8940–8951. doi:10.1523/JNEUROSCI.0026-12.2012. [PubMed: 22745494]

Hasson U. Intersubject Synchronization of Cortical Activity During Natural Vision. Science. 2004; 303:1634–1640. doi:10.1126/science.1089506. [PubMed: 15016991]

Herman P, Sanganahalli BG, Blumenfeld H, Hyder F. Cerebral oxygen demand for short-lived and steady-state events. J. Neurochem. 2009; 109:73–79. doi:10.1111/j.1471-4159.2009.05844.x. [PubMed: 19393011]

Hillman EMC, Devor A, Bouchard MB, Dunn AK, Krauss GW, Skoch J, Bacskai BJ, Dale AM, Boas DA. Depth-resolved optical imaging and microscopy of vascular compartment dynamics during somatosensory stimulation. NeuroImage. 2007; 35:89–104. doi:10.1016/j.neuroimage. 2006.11.032. [PubMed: 17222567]

Hoge RD, Atkinson J, Gill B, Crelier GR, Marrett S, Pike GB. Stimulus-dependent BOLD and perfusion dynamics in human V1. NeuroImage. 1999; 9:573–585. doi:10.1006/nimg.1999.0443. [PubMed: 10334901]

Iadecola C. Neurovascular regulation in the normal brain and in Alzheimer's disease. Nat Rev Neurosci. 2004; 5:347–360. doi:10.1038/nrn1387. [PubMed: 15100718]

Kasischke KA. Neural Activity Triggers Neuronal Oxidative Metabolism Followed by Astrocytic Glycolysis. Science. 2004; 305:99–103. doi:10.1126/science.1096485. [PubMed: 15232110]

Kim T, Kim S-G. Temporal dynamics and spatial specificity of arterial and venous blood volume changes during visual stimulation: implication for BOLD quantification. Journal of Cerebral Blood Flow & Metabolism. 2010; 31:1211–1222. doi:10.1038/jcbfm.2010.226. [PubMed: 21179068]

Leenders KL, Perani D, Lammertsma AA, Heather JD, Buckingham P, Healy MJ, Gibbs JM, Wise RJ, Hatazawa J, Herold S. Cerebral blood flow, blood volume and oxygen utilization. Normal values and effect of age. Brain. 1990; 113:27–47. Pt 1. [PubMed: 2302536]

Liang CL, Ances BM, Perthen JE, Moradi F, Liau J, Buracas GT, Hopkins SR, Buxton RB. Luminance contrast of a visual stimulus modulates the BOLD response more than the cerebral blood flow response in the human brain. NeuroImage. 2013; 64:104–111. doi:10.1016/j.neuroimage.2012.08.077. [PubMed: 22963855]

Liu TT, Wong EC. A signal processing model for arterial spin labeling functional MRI. NeuroImage. 2005; 24:207–215. doi:10.1016/j.neuroimage.2004.09.047. [PubMed: 15588612]

Logothetis NK. What we can do and what we cannot do with fMRI. Nature. 2008; 453:869–878. doi: 10.1038/nature06976. [PubMed: 18548064]

Lu H, Golay X, Pekar JJ, van Zijl PCM. Sustained Poststimulus Elevation in Cerebral Oxygen Utilization After Vascular Recovery. Journal of Cerebral Blood Flow & Metabolism. 2004; 24:764–770. doi:10.1097/01.WCB.0000124322.60992.5C. [PubMed: 15241184]

Malonek D, Grinvald A. Interactions between electrical activity and cortical microcirculation revealed by imaging spectroscopy: implications for functional brain mapping. Science. 1996; 272:551–554. [PubMed: 8614805]

Moradi F, Buracas GT, Buxton RB. Attention strongly increases oxygen metabolic response to stimulus in primary visual cortex. NeuroImage. 2012; 59:601–607. doi:10.1016/j.neuroimage. 2011.07.078. [PubMed: 21839179]

Moradi F, Buxton RB. Adaptation of cerebral oxygen metabolism and blood flow and modulation of neurovascular coupling with prolonged stimulation in human visual cortex. NeuroImage. 2013; 82:182–189. doi:10.1016/j.neuroimage.2013.05.110. [PubMed: 23732885]

Niazy RK, Xie J, Miller K, Beckmann CF, Smith SM. Spectral characteristics of resting state networks. Prog. Brain Res. 2011; 193:259–276. doi:10.1016/B978-0-444-53839-0.00017-X. [PubMed: 21854968]

Noll DC, Fessler JA, Sutton BP. Conjugate phase MRI reconstruction with spatially variant sample density correction. IEEE Trans. Med. Imaging. 2005; 24:325–336. doi:10.1109/TMI.2004.842452. [PubMed: 15754983]

Obata T, Liu TT, Miller KL, Luh W-M, Wong EC, Frank LR, Buxton RB. Discrepancies between BOLD and flow dynamics in primary and supplementary motor areas: application of the balloon model to the interpretation of BOLD transients. NeuroImage. 2004; 21:144–153. doi:10.1016/j.neuroimage.2003.08.040. [PubMed: 14741651]

Ogawa S, Tank DW, Menon R, Ellermann JM, Kim SG, Merkle H, Ugurbil K. Intrinsic signal changes accompanying sensory stimulation: functional brain mapping with magnetic resonance imaging. Proc. Natl. Acad. Sci. U.S.A. 1992; 89:5951–5955. [PubMed: 1631079]

Pelli DG. The VideoToolbox software for visual psychophysics: transforming numbers into movies. Spat Vis. 1997; 10:437–442. [PubMed: 9176953]

Perthen JE, Lansing AE, Liau J, Liu TT, Buxton RB. Caffeine-induced uncoupling of cerebral blood flow and oxygen metabolism: A calibrated BOLD fMRI study. NeuroImage. 2008; 40:237–247. doi:10.1016/j.neuroimage.2007.10.049. [PubMed: 18191583]

Restom K, Behzadi Y, Liu TT. Physiological noise reduction for arterial spin labeling functional MRI. NeuroImage. 2006; 31:1104–1115. doi:10.1016/j.neuroimage.2006.01.026. [PubMed: 16533609]

Simon AB, Griffeth VEM, Wong EC, Buxton RB. A Novel Method of Combining Blood Oxygenation and Blood Flow Sensitive Magnetic Resonance Imaging Techniques to Measure the Cerebral Blood Flow and Oxygen Metabolism Responses to an Unknown Neural Stimulus. PLoS ONE. 2013; 8:e54816. doi:10.1371/journal.pone.0054816.s003. [PubMed: 23382977]

Smith SM, Fox PT, Miller KL, Glahn DC, Fox PM, Mackay CE, Filippini N, Watkins KE, Toro R, Laird AR. Correspondence of the brain's functional architecture during activation and rest. Proc. Natl. Acad. Sci. U.S.A. 2009; 106:13040–13045. [PubMed: 19620724]

Snyder AZ, Raichle ME. A brief history of the resting state: The Washington University perspective. NeuroImage. 2012; 62:902–910. doi:10.1016/j.neuroimage.2012.01.044. [PubMed: 22266172]

Vazquez AL, Fukuda M, Kim S-G. Evolution of the dynamic changes in functional cerebral oxidative metabolism from tissue mitochondria to blood oxygen. Journal of Cerebral Blood Flow & Metabolism. 2012; 32:745–758. doi:10.1038/jcbfm.2011.198. [PubMed: 22293987]

Wong EC, Buxton RB, Frank LR. Quantitative imaging of perfusion using a single subtraction (QUIPSS and QUIPSS II). Magn. Reson. Med. 1998; 39:702–708. [PubMed: 9581600]

Highlights

- Dynamic coupling of CBF, CMRO2 and CBVv tested with contrast-oscillating stimulus.

- Envelope of BOLD but not CBF response characterized by slow decay in amplitude.

- Relationship between BOLD and CBF oscillations showed no evidence of hysteresis.

- Trajectory of BOLD and CBF oscillations did not pass through pre-stimulus baseline.

- BOLD/CBF responses suggest tight CBF/CMRO2 coupling with slow venous CBV response.
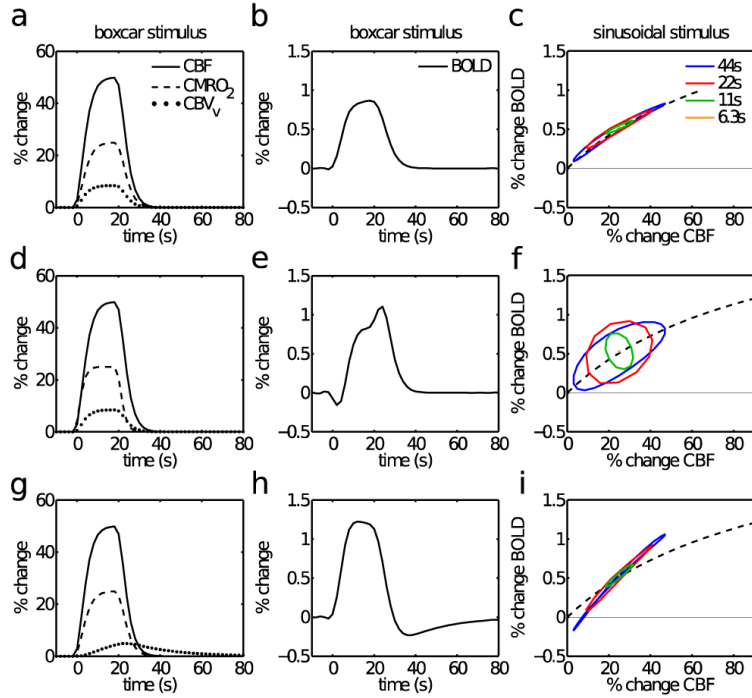
Figure 1. Characteristic simulated responses to boxcar and sinusoidal stimuli for coupled or decoupled physiological response dynamics

Top row (a-c): responses to boxcar and sinusoidal stimuli assuming tight coupling of CBF, $CMRO_2$, and CBV_v dynamics. Middle row (d-f): responses assuming fast $CMRO_2$ dynamics, producing an 'initial dip' in BOLD response to a boxcar stimulus. Bottom row (g-i): Responses assuming slow CBV_v dynamics, producing a 'post-stimulus undershoot' in BOLD response to a boxcar stimulus. Left column (a,d,g): physiological responses to boxcar stimulus. Middle column (b,e,h): BOLD responses to boxcar stimulus. Right column (c,f,i): relationship between BOLD and CBF responses to continuous stimulation during which contrast is oscillating with period of 44s, 22s, 11s, or 6.3s. The black dashed line represents the BOLD-CBF relationship predicted by Equation 1.
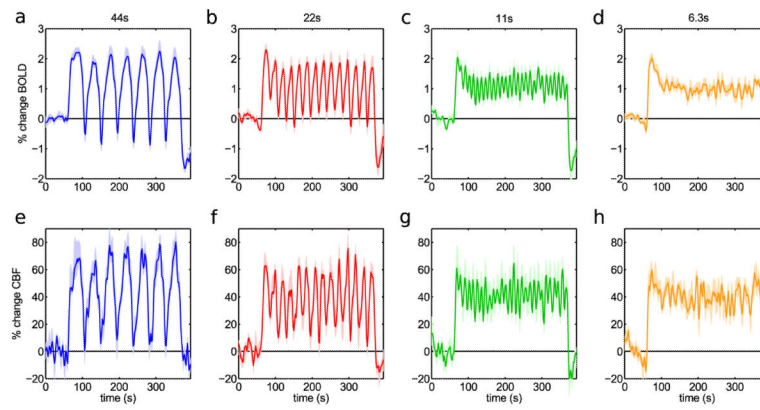
Figure 2. CBF and BOLD responses to contrast-oscillating visual stimuli

The top row displays the BOLD responses to each stimulus, averaged across subjects, while the bottom row displays the CBF responses. Responses are displayed as the percentage change from their baseline values before the start of the stimulus. Blue indicates the response to the 44s period stimulus, red - the response to the 22s stimulus, green – the response to the 11s stimulus, and orange - the response to the 6.3s stimulus. The stimulus begins at t=60s and ends at t = 368s. Shaded area represents +/− 1 standard error of the mean.
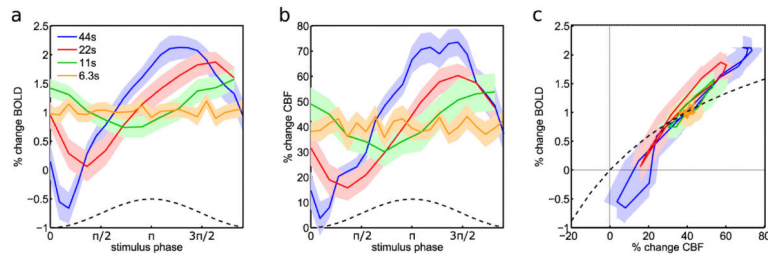
Figure 3. BOLD and CBF responses to contrast-oscillating stimuli averaged over a stimulus cycle
(a) Average BOLD responses over a contrast-oscillation cycle. The lightly shaded area indicates the region within one standard error of the mean across subjects. The dashed black line indicates the relative contrast of the stimulus. (b) Average CBF responses over a contrast-oscillation cycle. (c) Relationship between BOLD and CBF responses over stimulus cycle. All BOLD and CBF responses are displayed as the percentage change from their baseline values before the start of the stimulus. The dashed black line indicates the BOLD-CBF relationship corresponding to constant CBF-CMRO$_2$ and CBF-CBV$_v$ coupling.
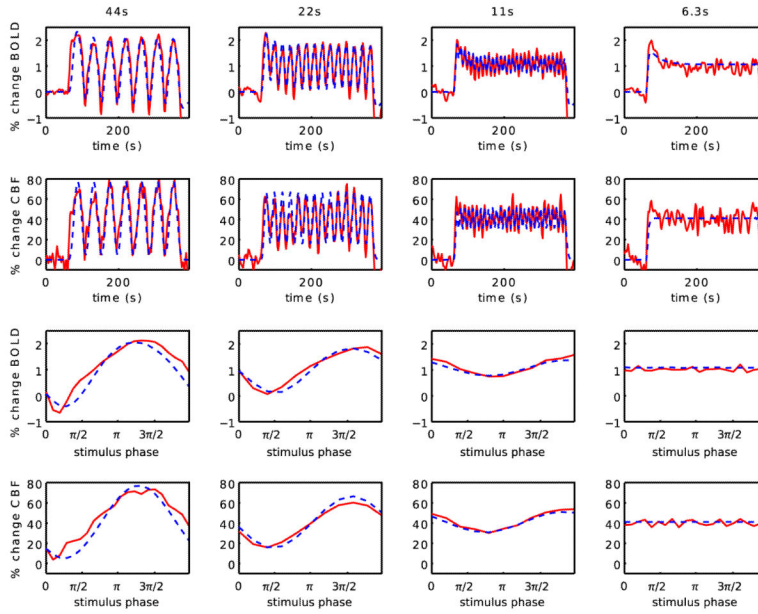
Figure 4. Comparison of simulated CBF and BOLD responses to contrast-oscillating stimuli with measured responses

Top row: measured (red) and simulated (dashed blue) BOLD responses. Second row: measured and simulated CBF responses. Third row: measured and simulated BOLD responses averaged over a single stimulus cycle. Bottom row: measured and simulated CBF responses averaged over a single stimulus cycle. All measured BOLD and CBF responses are averaged across subjects and displayed as the percentage change from their baseline values before the start of the stimulus.
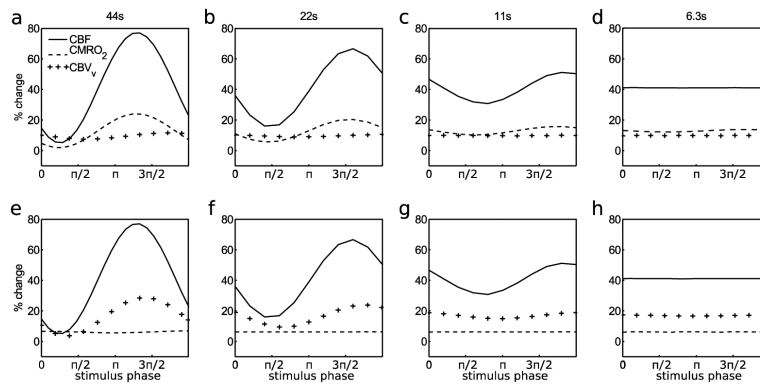
Figure 5. Simulated CBF, CMRO$_2$ and, CBV$_v$ responses over single stimulation cycle
Records reflect the responses after a prolonged period of stimulation such that slow components have had time to respond. Top row: simulated responses for case in which CBV$_v$ dynamics are slow compared to CBF and CMRO$_2$. Bottom row: simulated responses for the case in which CMRO$_2$ dynamics are slow compared to CBF and CBV$_v$. All responses are displayed as the percentage change from their baseline values before the start of the stimulus.

Table 1

Description of dynamic model parameters.

Parameter	Description	Value[s]
$q(t)$	Ratio of deoxyhemoglobin quantity at time t to baseline	Variable
$r(t)$	Ratio of CMRO2 at time t to baseline	Variable
$f_{in}(t)$	Ratio of CBF inflow at time t to baseline	Variable
$f_{out}(t)$	Ratio of CBF outflow at time t to baseline	Variable
$v(t)$	Ratio of venous CBV at time t to baseline	Variable
$c(t)$	Stimulus contrast at time t	Variable
$h(t)_{f,r}$	Convolution kernel relating CBF and CMRO2 to stimulus contrast	Variable
$H_{f,r}$	Scaling parameter for CBF and CMRO2 convolution kernels	Variable
α_v	Exponent describing steady state venous flow-volume coupling	Variable
$\tau_{v,f,r}$	Characteristic time constants for venous CBV, CBF and CMRO2	Variable
τ_0	Transit time for blood through venous compartment	2s [0.75s-2.5s]
z	Shape parameter for CBF and CMRO2 convolution kernels	3 [2-4]
ψ	BOLD-deoxyhemoglobin scaling constant	3 [2-7]